PHILOSOPHICAL TRANSACTIONS OF THE ROYAL SOCIETY A

*Phil. Trans. R. Soc. A* (2011) **369**, 4316–4330
doi:10.1098/rsta.2011.0130

# Virtual surgeries in patients with congenital heart disease: a multi-scale modelling test case

By A. Baretta[1], C. Corsini[1], W. Yang[2], I. E. Vignon-Clementel[3], A. L. Marsden[2], J. A. Feinstein[4], T.-Y. Hsia[5], G. Dubini[1], F. Migliavacca[1], G. Pennati[1,*] and the Modeling of Congenital Hearts Alliance (MOCHA) Investigators

[1]*Laboratory of Biological Structure Mechanics, Structural Engineering Department, Politecnico di Milano, Milan, Italy*
[2]*Mechanical and Aerospace Engineering Department, University of California San Diego, San Diego, CA, USA*
[3]*INRIA Paris-Rocquencourt, Le Chesnay, France*
[4]*Departments of Pediatrics and Bioengineering, Stanford University, Lucile Packard Children's Hospital, Palo Alto, CA, USA*
[5]*Institute of Child Health and Great Ormond Street Hospital for Children, London, UK*

The objective of this work is to perform a virtual planning of surgical repairs in patients with congenital heart diseases—to test the predictive capability of a closed-loop multi-scale model. As a first step, we reproduced the pre-operative state of a specific patient with a univentricular circulation and a bidirectional cavopulmonary anastomosis (BCPA), starting from the patient's clinical data. Namely, by adopting a closed-loop multi-scale approach, the boundary conditions at the inlet and outlet sections of the three-dimensional model were automatically calculated by a lumped parameter network. Successively, we simulated three alternative surgical designs of the total cavopulmonary connection (TCPC). In particular, a T-junction of the venae cavae to the pulmonary arteries (T-TCPC), a design with an offset between the venae cavae (O-TCPC) and a Y-graft design (Y-TCPC) were compared. A multi-scale closed-loop model consisting of a lumped parameter network representing the whole circulation and a patient-specific three-dimensional finite volume model of the BCPA with detailed pulmonary anatomy was built. The three TCPC alternatives were investigated in terms of energetics and haemodynamics. Effects of exercise were also investigated. Results showed that the pre-operative caval flows should not be used as boundary conditions in post-operative simulations owing to changes in the flow waveforms post-operatively. The multi-scale approach is a possible solution to overcome this incongruence. Power losses of the Y-TCPC were lower than all other TCPC models both at rest and under exercise conditions and it distributed the inferior vena cava flow evenly to both lungs. Further work is needed to correlate results from these simulations with clinical outcomes.

*Author for correspondence (giancarlo.pennati@polimi.it).

One contribution of 11 to a Theme Issue 'Towards the virtual physiological human: mathematical and computational case studies'.

 

**Keywords: mathematical models; patient-specific; congenital heart diseases; finite volume method; lumped parameter models**

## 1. Introduction

Cavopulmonary connections are surgical procedures used to treat a variety of complex congenital heart diseases. Such malformations, in which a patient has only one effective or functional cardiac pumping chamber (univentricular heart), are usually fatal within the first days or months of life unless treated surgically.

These 'single-ventricle' patients usually undergo a series of surgeries resulting in a 'Fontan circulation' [1] in which the single ventricle pumps blood returning from the lungs to the body, and the blood returning from the body travels passively to the lungs via direct blood vessel connections without a pumping chamber. This configuration, called a total cavopulmonary connection (TCPC) [2], is the result of a three-staged surgical series performed on single ventricle heart patients. In the TCPC, the superior vena cava (SVC) and the inferior vena cava (IVC) are directly connected to the right pulmonary artery (RPA), with the IVC connected via either an intra-atrial tunnel or extra cardiac conduit. The previous surgical step is the bidirectional cavopulmonary anastomosis (BCPA) that consists of the connection between the SVC and the RPA [3].

The T-junction configuration of the TCPC leads to unusual haemodynamic conditions that are not known to occur naturally in any region of the circulatory system. Computational modelling, clinical observation and experimental studies have suggested that the geometry of the TCPC plays a key role in energy losses and fluid dynamics [2,4] and previous work has considered both offset and Y-shaped alternative designs [5–7].

For this reason, most *in vitro* and *in silico* studies using simplified models have focused on local fluid dynamics, with a primary focus on energy dissipation resulting from different connection geometries. The goal of these studies was the geometrical optimization of the connections, in order to minimize the energy expenditure. Moreover, the caval flow distribution to the pulmonary arteries was investigated as an important parameter for patient outcomes and the development of arteriovenous malformations [8].

One of the main limitations of current computational fluid dynamics (CFD) models relates to the suitability of the inlet and outlet boundary conditions. Boundary conditions must correctly simulate the upstream and downstream fluid dynamics and control flow distribution among the various branches and vessels [9]. In the last decade, three-dimensional models of the cavopulmonary connection coupled to downstream impedances were adopted to assess the relative role played by local geometry and pulmonary vasculature without directly imposing pulmonary flow splits [5]. Nevertheless, such models result in an open-loop configuration where the inlet boundary conditions (flow or pressure) have to be imposed and the effects on global circulatory parameters cannot be determined.

More recently, this approach was applied to patient-specific models derived from magnetic resonance (MR) images and clinical measurements [9], with the intention of investigating the fluid dynamics in BCPA [10,11] and TCPC under realistic anatomical and boundary conditions [12–15]. Clinical measurements

(e.g. pressures and cardiac output) may be acquired at different times, using multiple methods and under varying and 'abnormal' conditions (e.g. supine, resting, sedated and intubated). These occurrences may lead to inconsistencies within the data to be used in simulations. Nevertheless, it is evident that such patient data cannot be available for predictive investigations of future scenarios. In particular, boundary conditions for models simulating post-operative haemodynamics cannot be clinically measured prior to the surgical operation. This results in an important limitation for virtual planning of cardiovascular repairs, since the pre-operative measured flow data are usually adopted as inlet boundary conditions for the post-operative simulations.

The aim and the novelty of this study are to perform a TCPC virtual planning using a closed-loop multi-scale modelling approach. The solution at both inlet and outlet boundaries of the detailed region under investigation is coupled with a lumped parameter model (LPM) of the remaining cardiovascular system. A multi-scale closed-loop approach was recently adopted to simulate haemodynamics in the coronary tree on the basis of a patient-specific three-dimensional model and a typical LPM description [16,17]. In the present work, the detailed region of the connections (BCPA and TCPC) is patient-specific and built from an MR scan; similarly, the LPM is customized using the patient's data pre-operatively collected. Different virtual post-operative scenarios are simulated to demonstrate the potential of this methodology. In particular, three TCPC configurations are investigated under rest and exercise conditions.

## 2. Material and methods

### (*a*) *Clinical data*

The patient analysed for this test case was a 4-year-old male patient (Lucile Packard Children's Hospital, Stanford, CA, USA), who had undergone a BCPA. The clinical data used for the present study were acquired a month before he underwent the TCPC. MR digital imaging and communications in medicine images were used to build the BCPA geometry, and the haemodynamic data consisted of MR flow tracings, catheterization-derived pressure tracings and echocardiographic Doppler velocity tracings (figure 1*a*). All clinical data are listed in table 1.

Patient right pulmonary (RPVR) and left pulmonary (LPVR) and upper body (UBSVR) and lower body (LBSVR) systemic vascular resistances (SVRs) were calculated on the basis of mean values of pressures and flows as follows:

$$\mathrm{RPVR} = \frac{P_{\mathrm{SVC}} - P_{\mathrm{atrium}}}{Q_{\mathrm{p-R}}}, \tag{2.1}$$

$$\mathrm{LPVR} = \frac{P_{\mathrm{SVC}} - P_{\mathrm{atrium}}}{Q_{\mathrm{p-L}}}, \tag{2.2}$$

$$\mathrm{UBSVR} = \frac{P_{\mathrm{arch}} - P_{\mathrm{SVC}}}{Q_{\mathrm{p}}} \tag{2.3}$$

and

$$\mathrm{LBSVR} = \frac{P_{\mathrm{arch}} - P_{\mathrm{atrium}}}{Q_{\mathrm{s}} - Q_{\mathrm{p}}}, \tag{2.4}$$

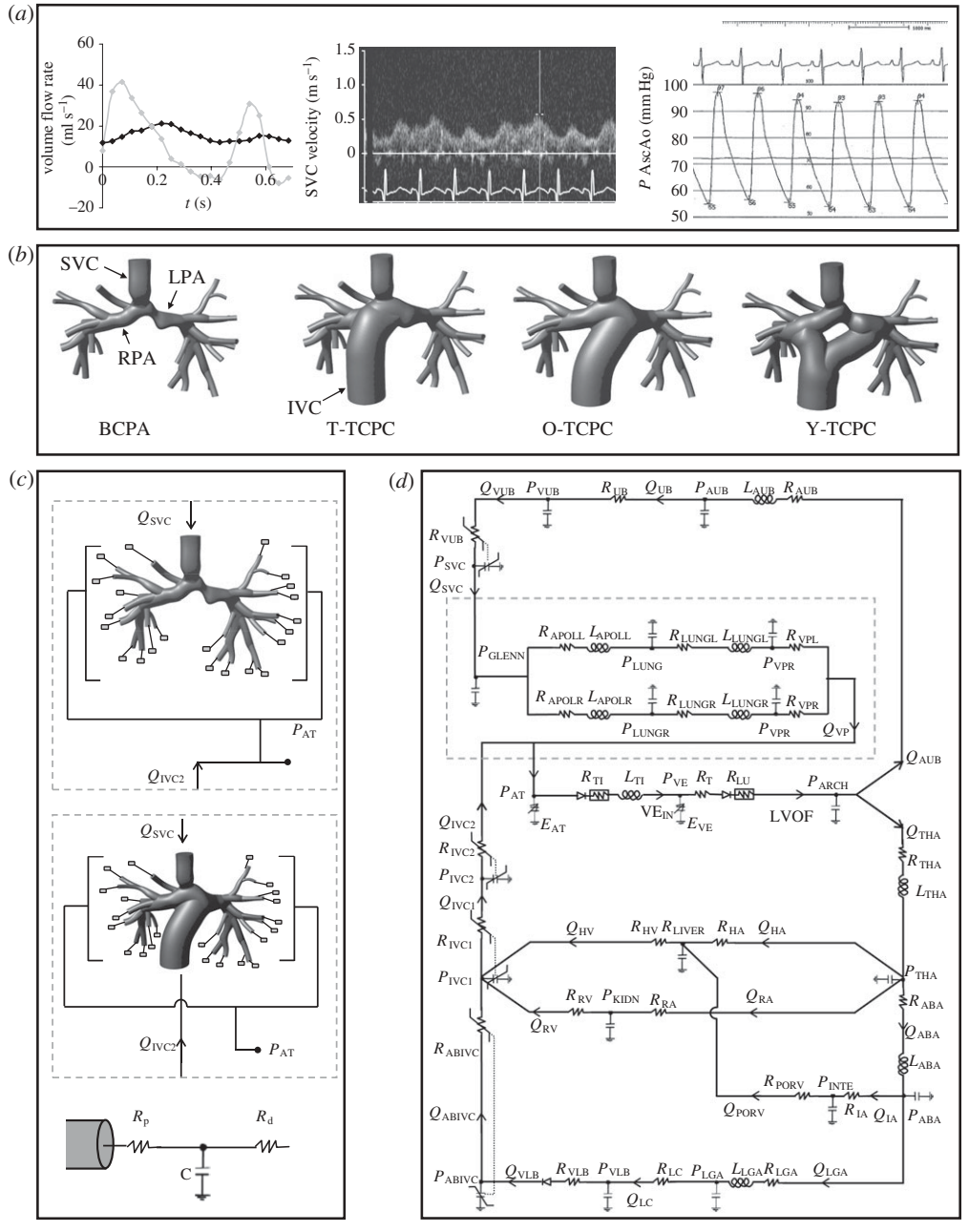


Figure 1. (*a*) Magnetic resonance flow waveforms measured in the venae cavae (left; black solid line, $Q_{\mathrm{SVC}}$; grey solid line, $Q_{\mathrm{IVC}}$), superior vena cava (SVC) velocity waveform measured with echo-Doppler ultrasound (centre) and pressure tracings measured with catheterization in the ascending aorta (right); (*b*) three-dimensional pre-operative model (BCPA) and post-operative models (T-TCPC, O-TCPC, Y-TCPC); (*c*) three-dimensional–zero-dimensional coupling of the pre-operative (top) and post-operative (centre) geometries with the pulmonary resistance–compliance–resistance blocks (bottom); and (*d*) lumped parameter model of the pre-operative circulation.

Table 1. Values of flow rates and pressures (maximum $M$, minimum $m$ and mean $\bar{m}$) from clinical data and for the BCPA LPM and the BCPA multi-scale model. CO, cardiac output; $Q$, flow rate; UB, upper body; LB, lower body; LPA, left pulmonary artery; RPA, right pulmonary artery; SVC, superior vena cava; IVC, inferior vena cava.

| | clinical data | | | BCPA LPM | | | multi-scale BCPA model | | |
|---|---|---|---|---|---|---|---|---|---|
| flows ($\mathrm{ml\,s^{-1}}$) | | | | | | | | | |
| CO | 28.86 | | | 28.56 | | | 28.11 | | |
| $Q_{\mathrm{UB}}$ ($Q_{\mathrm{SVC}}$) | 15.58 | | | 15.48 | | | 15.16 | | |
| $Q_{\mathrm{LB}}$ ($Q_{\mathrm{IVC}}$) | 13.27 | | | 13.08 | | | 12.95 | | |
| $Q_{\mathrm{LPA}}$ | 5.54 | | | 5.56 | | | 5.43 | | |
| $Q_{\mathrm{RPA}}$ | 10 | | | 9.92 | | | 9.73 | | |
| pressures (mm Hg) | $M$ | $m$ | $\bar{m}$ | $M$ | $m$ | $\bar{m}$ | $M$ | $m$ | $\bar{m}$ |
| ventricle | 94 | 8[a] | n.a. | 96 | 6.2[a] | 31.7 | 93.1 | 6[a] | 31.2 |
| atrium | n.a. | n.a. | 5 | 8.6 | 3.7 | 5.7 | 8.7 | 3.4 | 5.5 |
| aortic arch | 94 | 54 | 72 | 94.2 | 50.4 | 70.2 | 93 | 50 | 69.4 |
| LPA | 12 | 6 | 9 | 10.9 | 8.5 | 9.5 | 11.1 | 8.7 | 9.7 |
| RPA | 13 | 8 | 10 | 10.9 | 8.5 | 9.5 | 11.2 | 8.7 | 9.7 |
| SVC | 14 | 7 | 10 | 12.1 | 10.4 | 11 | 12.3 | 10.9 | 11.4 |

[a]End-diastolic pressures.

where $P_{\mathrm{SVC}}$, $P_{\mathrm{atrium}}$ and $P_{\mathrm{arch}}$ represent the SVC pressure, the atrial pressure and the aortic arch pressure, respectively. $Q_{\mathrm{p}}$ is the pulmonary (or SVC) flow, $Q_{\mathrm{p-R}}$ and $Q_{\mathrm{p-L}}$ are the right and left pulmonary flows and $Q_{\mathrm{s}}$ is the systemic flow (i.e. cardiac output). For the studied patient, RPVR, LPVR, UBSVR and LBSVR were equal to 8.3, 15, 64.2 and 81.6 mm Hg min $\mathrm{l^{-1}}$ (Woods units, WU; 1 WU = 7999.2 Pa s $\mathrm{l^{-1}}$), respectively. Total pulmonary vascular resistance in the studied patient was 5.3 WU and the SVR was 35 WU.

### (*b*) *Three-dimensional models of cavopulmonary connections and resistance–compliance–resistance* (*RCR*) *blocks*

The geometrical three-dimensional model of the pre-operative anatomy, representing the BCPA, was created from MR images using SimVascular (http://simtk.org) [9] and is depicted in figure 1*b*.

The BCPA model includes the SVC, the RPA and the left pulmonary artery (LPA) and 22 pulmonary branches, with 10 RPA outlets and 12 LPA outlets. A stenosis in the proximal region of the LPA can also be observed. The three-dimensional model has an SVC inlet diameter of 11.6 mm, while the outlet diameters range between 1.8 and 4.5 mm.

Using virtual surgery techniques with the same software [15,18], three different TCPC configurations were created (figure 1*b*): a traditional T-junction with no offset between the venae cavae (T-TCPC), a configuration with an offset towards the LPA (O-TCPC) and a Y-graft connection with 15 mm branches (Y-TCPC) [7,19]. For all of the models, the IVC-graft diameter is equal to 20 mm, in agreement with standard surgical practice. It should be noted that the pre-operative geometry was modified to create the T- and O-junction, so that the

stenosis in the LPA was alleviated. The stenosis is still present in the Y-graft model, but the IVC bifurcation allows the flow to by-pass it. In all the models, the SVC and pulmonary artery portions are identical in the pre- and post-operative models.

Using Ansys ICEM 12.1 (Ansys Inc., Canonsburg, PA, USA), the models were discretized with tetrahedral elements and a grid sensitivity analysis was carried out, progressively increasing the mesh density. In agreement with preliminary CFD simulations (Fluent 12.1, Ansys Inc.), a mesh size of approximately 640 000 and 720 000 for the BCPA and TCPC models, respectively, was found to achieve mesh independence for the quantities of interest (namely, the pressure drop between the inlets and the outlets), and an acceptable CPU time expenditure.

The patient-specific downstream boundary conditions at the pulmonary artery branch outlets of the three-dimensional models were prescribed using RCR impedance blocks (figure 1*c*), whose values were estimated to best match available pre-operative clinical data (transpulmonary pressure gradient and right/left lung blood flow split to compute the total resistance for each branch) and morphometric pulmonary artery data (proximal and distal resistances, capacitance) [20] as described in detail in Troianowski *et al.* [11].

### (*c*) *Pre-operative lumped parameter model of the patient cardiovascular system*

An LPM of the whole cardiovascular system (heart, systemic and pulmonary circulations) for the BCPA case was developed based on our previous work [21,22].

The BCPA network comprises 21 blocks: 13 to represent the systemic circulation, six for the pulmonary circulation and two for each abdominal organ (liver, intestine and kidneys) as depicted in figure 1*d*. Venous valves were also included in the model by means of diodes in the leg venous blocks. Furthermore, the dependence of the great vein (SVC and IVC) resistances on transmural pressure was taken into account. Here, coronary circulation, gravity and respiratory effects were neglected. The heart was described by two time-varying elastances, a single atrium and a single ventricle, respectively. Their contractions were ruled by two activation functions, an atrial one and a ventricular one, shifted in time. Atrioventricular and aortic valves were described by nonlinear diodes. For more details, refer to Migliavacca *et al.* [23].

The parameter assessment of the BCPA model was made by first setting the patient's body surface area (BSA equal to $0.66\,\mathrm{m}^2$), heart rate (84 bpm) and RPVR, LPVR, UBSVR and LBSVR values.

The effect of the patient's BSA was included by making use of allometric equations [24], where model parameters are scaled according to proper powers of the BSA specific for the various vascular districts or organs [25]:

$$x = x_0 \left( \frac{\mathrm{BSA}}{\mathrm{BSA}_0} \right)^b, \tag{2.5}$$

where $x$ and $x_0$ are the vascular ($R$, $C$ and $L$) and heart ($R_{\mathrm{valve}}$, $L_{\mathrm{valve}}$ and elastances) parameters for the patient BSA and for a reference body surface area $\mathrm{BSA}_0$, respectively. The exponent $b$ is the 'scaling factor' and describes the effect of a change in the body size. $x_0$ values corresponding to an adult subject ($\mathrm{BSA}_0$ of $1.8\,\mathrm{m}^2$) were derived from Snyder & Rideout [26]. This procedure allowed us to set

Table 2. Values of $b$ coefficient of equation (2.5) adopted for the lumped parameters of the model. AUB, upper body arteries; UB, upper body capillaries; VUB, upper body veins; ABA, abdominal aorta; THA, thoracic aorta; ABIVC, abdominal inferior vena cava; IVC1(2), thoracic inferior vena cava 1(2); SVC, superior vena cava; APOLL(R), left (right) pulmonary arteries; LUNGL(R), left (right) arterioles and venules; VPL(R), left (right) pulmonary vein; HA, hepatic artery; HV, hepatic vein; RA, renal artery; RV, renal vein; IA, iliac artery; PORV, portal vein; AT, atrium; TI, atrioventricular valve; T, myocardial viscous resistance; LU, semilunar valve; LGA, leg arteries; LC, leg capillaries; VLB, leg veins.

| blocks | $R$ | $C$ | $L$ |
|---|---|---|---|
| AUB, UB, VUB | −0.3 | 0.4 | −0.1 |
| ABA, THA, ABIVC, IVC1, IVC2, SVC, APOLL, APOLR, LUNGL, LUNGR, VPL, VPR, HA, HV, RA, RV, IA, PORV | −0.9 | 1.2 | −0.3 |
| AT, TI, T, LU | −1.2 | 0.5 | −0.3 |
| LGA, LC, VLB | −1.86 | 2.48 | −0.3 |

a model for a generic $0.66\,\mathrm{m}^2$ subject, having resistance $R_{\mathrm{i-BSA}}$ and compliance $C_{\mathrm{i-BSA}}$ for the i-block. Table 2 reports the $b$ coefficients for all the adopted lumped parameters.

Moreover, the patient-specific information on vascular resistances (RPVR, LPVR, UBSVR and LBSVR) was used to fine tune the resistive model parameters. Then, the patient-specific compliance values of each vascular district were obtained as follows:

$$C_{\mathrm{i}} = C_{\mathrm{i\text{-}BSA}} \left( \frac{R_{\mathrm{i}}}{R_{\mathrm{i\text{-}BSA}}} \right)^{-4/3}, \tag{2.6}$$

where $R_{\mathrm{i}}$ indicates the patient-specific resistance evaluated for the i-block. The adopted power $(-4/3)$ accounts for the different dependence of the vascular resistances and compliances on vessels' dimensions ($R \approx l \cdot r^{-4}$ and $C \approx l \cdot r^{3}$, $r$ and $l$ being the radius and the length of a vessel, respectively [24]).

At this stage, the pre-operative LPM of the investigated clinical case was completed. Hence, pre-operative pressure and flow tracings were obtained, solving the algebraic-differential equation system describing the cardiovascular network by means of Simnon (version 3.00.011, 1998, SSPA Maritime Consulting, Göteborg, Sweden), with the 4th/5th order Runge–Kutta–Fehlberg numerical method (RKF-4th/5th), and an integration time of 0.0005 s.

### (*d*) *Closed-loop multi-scale models*

Multi-scale BCPA and TCPC models were built starting from the pre-operative LPM, in which the pulmonary region was substituted by each three-dimensional model and the RCR blocks (pulmonary impedances; figure 1*c*). The three-dimensional geometry was imported in ANSYS Fluent 12.1 and the three-dimensional–LPM coupling was performed by means of user-defined functions written in C++ language as described in Migliavacca *et al.* [27]. The exchange of pressure and flow information was made at the three-dimensional domain boundary sections once per time step. The zero-dimensional model passes

pressures at the boundaries to the three-dimensional model, where the Navier–Stokes equations are solved. Flow rates are computed at the boundaries of the three-dimensional model, and passed as an input to the zero-dimensional model. The BCPA multi-scale simulations were initialized with values of pressures and flows derived from previous simulations run with the stand-alone LPM. The LPM was in turn initialized with reasonable values of pressures and flows derived from the literature. This leads three-dimensional–zero-dimensional simulations to faster reach periodicity (in three cardiac cycles).

Transient simulations for each model were run on an IntelR Core i7 (3 GHz) processor, with a 64 bit operating system. The ordinary differential equation system resulting from the LPM was solved with the explicit Euler method, using a time step of 0.0005 s. The multi-scale simulations required a CPU time expenditure of approximately 1.5 days per cardiac cycle. The blood was assumed to be a Newtonian fluid, with a viscosity of $0.004\,\mathrm{kg\,m\,s^{-1}}$ and a density of $1060\,\mathrm{kg\,m^{-3}}$. No gravitational effects were taken into account. Rigid walls were assumed for the three-dimensional portion of the model.

The BCPA model was tested in rest conditions, similar to the patient's condition during a clinical examination, whereas rest and exercise conditions were simulated for all the TCPC models, in order to evaluate the performances of the different configurations over a range of conditions. Exercise conditions were obtained by doubling the heart rate, reducing both LPVR and RPVR by 40 per cent [14], and the whole SVR by 33 per cent [28]. The decrease in SVR was obtained by reducing leg resistances by 85 per cent.

## 3. Results and discussion

### (a) *Pre-operative lumped parameter model*

After setting the heart rate, the body surface area and the resistances on the basis of the measured PVR and SVR, the LPM of the BCPA circulation produced pressures and flows that match the clinical ones (table 1). Averaged values throughout a cardiac cycle of fluid dynamics variables calculated by model simulations show differences of less than 3 per cent from the corresponding clinical data.

In addition, the temporal flow waveforms are well captured by the model, thus proving the good quality of the model. As an example, the predicted waveforms of the caval (IVC and SVC) and pulmonary (LPA and RPA) flows are reported in figure 2 and compared with corresponding clinical flow waveforms. The different oscillations of flow in the two venae cavae are well predicted and the peculiar shape of the IVC flow (owing to the pressure changes in the atrium) is properly described, even if some discrepancies are visible during atrial contraction (approx. 0.4 s). The differences in the first 0.1 s are probably owing to the heart timing.

### (b) *Multi-scale bidirectional cavopulmonary anastomosis and total cavopulmonary connection models*

Comparing the BCPA multi-scale model and the LPM results, only small differences in mean values of flows are observed (less than 1%, table 1), whereas some variation occurred in the flow oscillations (figure 2). Maximum, minimum

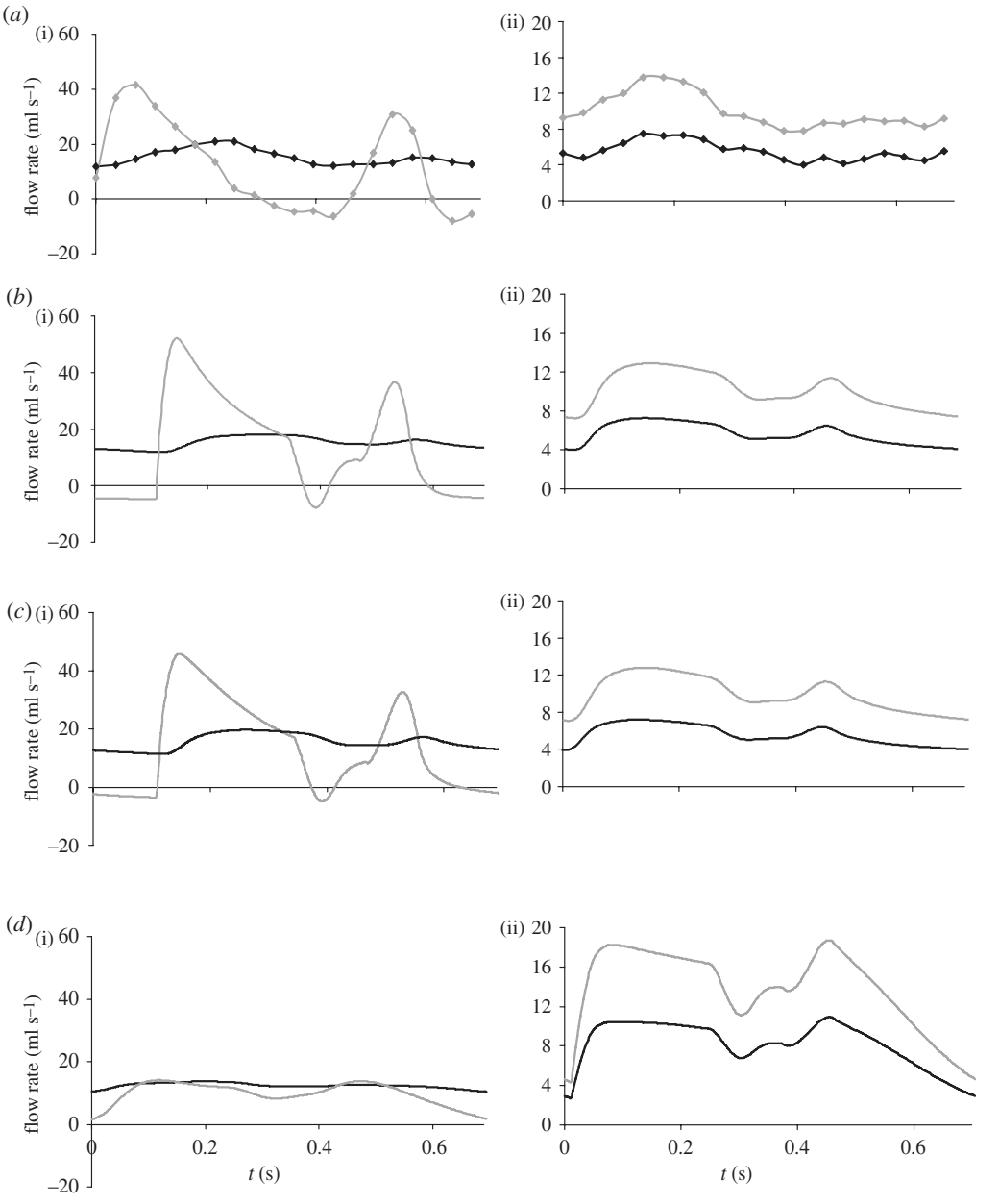


Figure 2. Caval ($a$(i)–$d$(i)) and pulmonary ($a$(ii)–$d$(ii)) volumetric flow rates obtained from: ($a$) the patient's MR data; ($b$) the BCPA LPM; ($c$) the BCPA multi-scale model and ($d$) the O-TCPC multi-scale model, as a representative of the post-operative models. ($a$)(i) Black diamonds with solid line, QSVC-MRI; grey diamonds with solid line, QIVC-MRI; (ii) grey diamonds with solid line, QRPA-MRI; black diamonds with solid line, QLPA-MRI. ($b$)(i) Black solid line, QSVC LPM; grey solid line, QIVC LPM; (ii) black solid line, QLPA LPM; grey solid line, QRPA LPM. ($c$)(i) Black solid line, QSVC multi-scale; grey solid line, QIVC multi-scale; (ii) black solid line, QLPA multi-scale; grey solid line, QRPA multi-scale. ($d$)(i) Black solid line, QSVC TCPC; grey solid line, QIVC TCPC; (ii) black solid line, QLPA TCPC; grey solid line, QRPA TCPC.

and mean values of pressures reasonably reproduce the LPM ones, as illustrated in table 1, with higher discrepancy than flow values, owing to the different conditions under which pressure data were acquired, i.e. mechanical ventilation. These differences are mainly owing to a reduction in the pulmonary vascular compliance since the three-dimensional model is rigid.

Results obtained from all the TCPC multi-scale models in rest conditions show comparable variations in global haemodynamic parameters with respect to the BCPA model. The caval flows decrease approximately 25 per cent, with an evident reduction in IVC pulsatility. Unfortunately, no post-operative data were collected for the investigated patient, owing to the invasiveness of such exams and the absence of necessity for clinical aims. Nevertheless, the predicted changes in caval flows are in a fairly good agreement with a previous study of ours [29], where MR caval flows were exceptionally acquired both pre- and post-operatively in a patient who underwent a TCPC surgery. Additionally, as the IVC has been disconnected from the contracting right atrium, reduced pulsatility in the IVC waveform is expected post-operatively. Hence, imposing inlet flows in the TCPC models equal to the pre-operatively measured caval flows [14] would have not been accurate. In a more recent study, Marsden and co-workers [15] constructed post-operative boundary conditions of an open-loop TCPC configuration using pre-operatively measured IVC flow, but with scaled-down amplitude to reduce cardiac pulsatility based on typical Fontan data. Nevertheless, the mean caval flow rates were preserved from pre-operative to post-operative state. In the present study, the changes in both SVC (decrease of mean flow rate) and IVC (decrease of mean flow rate and pulsatility) were directly evaluated by the closed-loop model, enhancing the importance of adopting such a multi-scale methodology.

In the exercise conditions, as a consequence of the imposed changes in heart rate and vascular resistances, the IVC flows in all the TCPC models are much higher than those at rest condition (approx. 23 versus $9.5\,\mathrm{ml\,s^{-1}}$), while the SVC flow is only slightly increased (by approx. 20%; table 3). It should be noted that these values are a result of the multi-scale model and they are not assumed as inlet conditions. In this regard, it is also interesting to observe the pre- and post-operative pressure–volume ($P$–$V$) loop during a cardiac cycle (figure 3) either at rest or under exercise conditions. The TCPC models report a $P$–$V$ curve shifted towards lower volumes and pressure suggesting that the final surgery (the TCPC) decreases the heart workload. Moreover, the stroke volume slightly decreases during exercise despite an increase in systolic pressure (CO is higher than at rest since heart rate was doubled).

Comparing the TCPC configurations in terms of local fluid dynamics and energy efficiency, some observations can be outlined. Either at rest or under exercise conditions, mean flow rate values differ by less than 1 per cent. Observing pathlines during peak IVC flow (figure 4), stagnation zones can be seen in the central region of the T-TCPC model, with SVC and IVC flows preferentially directed towards the LPA and RPA, respectively. Minor extension of such regions is shown in the O-TCPC model. For the Y-TCPC model, a wide stagnation zone downstream of the LPA–SVC connection can be detected. Moreover, from a qualitative point of view, IVC pathlines in the Y-TCPC and O-TCPC models are distributed to both lungs. A more balanced distribution of hepatic factor present in the IVC flow could avoid ‘long-term’ generation of arteriovenous malformations.

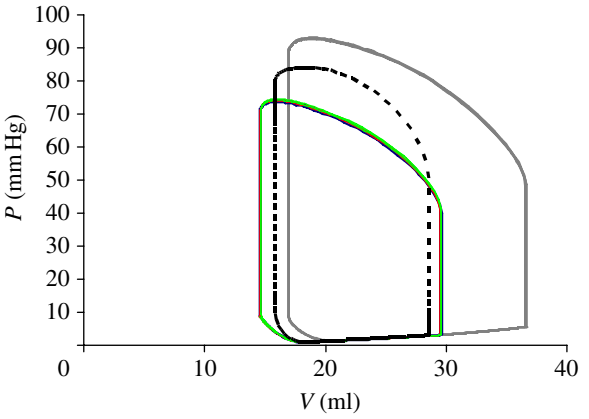


Figure 3. Ventricular pressure–volume loops at rest conditions for the pre- and post-operative models, and under exercise conditions (TCPC EXE) for the offset model. Grey solid line, BCPA; blue solid line, T-TCPC; red solid line, O-TCPC; green solid line, Y-TCPC; grey dashed line, TCPC EXE. (Online version in colour.)

Table 3. Values of flow rates, power loss and energy efficiency for the TCPC multi-scale models at rest and under exercise conditions. CO, cardiac output; $Q$, flow rate; UB, upper body; LB, lower body; LPA, left pulmonary artery; RPA, right pulmonary artery; SVC, superior vena cava; IVC, inferior vena cava; $P_{\mathrm{DISS}}$, power loss; $P_{\mathrm{effic}}$, energy efficiency.

| | multi-scale T-TCPC | multi-scale O-TCPC | multi-scale Y-TCPC |
|---|---|---|---|
| rest conditions | | | |
| CO ($\mathrm{ml\,s^{-1}}$) | 21.20 | 21.09 | 21.18 |
| $Q_{\mathrm{UB}}$ ($Q_{\mathrm{SVC}}$; $\mathrm{ml\,s^{-1}}$) | 11.45 | 11.52 | 11.56 |
| $Q_{\mathrm{LB}}$ ($Q_{\mathrm{IVC}}$; $\mathrm{ml\,s^{-1}}$) | 9.57 | 9.54 | 9.59 |
| $Q_{\mathrm{LPA}}$ ($\mathrm{ml\,s^{-1}}$) | 7.87 | 7.94 | 7.93 |
| $Q_{\mathrm{RPA}}$ ($\mathrm{ml\,s^{-1}}$) | 13.33 | 13.24 | 13.35 |
| $P_{\mathrm{DISS}}$ (mW) | 1.54 | 1.46 | 1.09 |
| $P_{\mathrm{effic}}$ (%) | 94.4 | 95.1 | 96.4 |
| exercise conditions | | | |
| CO ($\mathrm{ml\,s^{-1}}$) | 37.45 | 37.10 | 37.62 |
| $Q_{\mathrm{UB}}$ ($Q_{\mathrm{SVC}}$; $\mathrm{ml\,s^{-1}}$) | 14.04 | 13.75 | 14.12 |
| $Q_{\mathrm{LB}}$ ($Q_{\mathrm{IVC}}$; $\mathrm{ml\,s^{-1}}$) | 23.41 | 23.35 | 23.50 |
| $Q_{\mathrm{LPA}}$ ($\mathrm{ml\,s^{-1}}$) | 14.17 | 14.06 | 14.19 |
| $Q_{\mathrm{RPA}}$ ($\mathrm{ml\,s^{-1}}$) | 23.28 | 23.04 | 23.43 |
| $P_{\mathrm{DISS}}$ (mW) | 4.80 | 4.36 | 3.37 |
| $P_{\mathrm{effic}}$ (%) | 91.9 | 92.7 | 94.4 |

From table 3, the T-TCPC model reports the lowest energy efficiency if compared with the other models (94.4% at rest and 91.9% at exercise), corresponding to the highest power losses (1.54 mW at rest and 4.80 mW at exercise). The Y-TCPC model showed the highest efficiency under rest (96.4%) and exercise (94.4%) conditions, which is related to lower power loss values (1.09 mW at rest and 3.37 mW at exercise), despite the remaining stenosis.

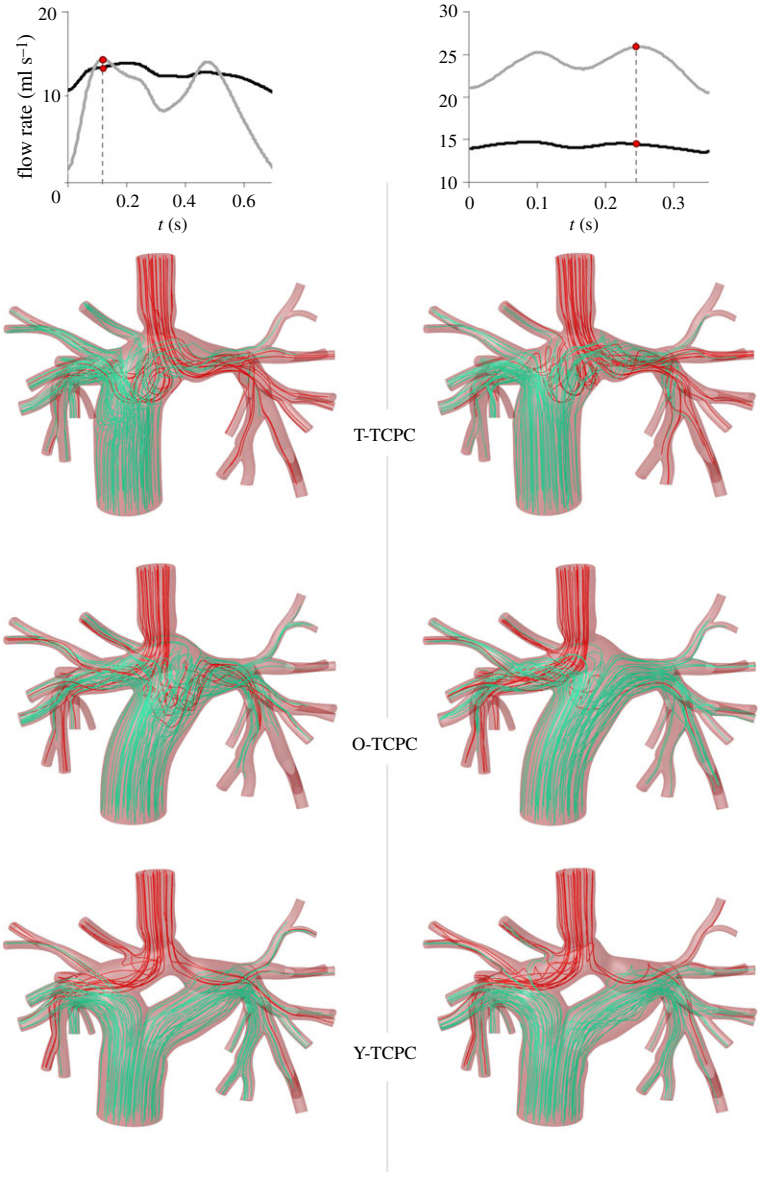


Figure 4. SVC and IVC pathlines during peak IVC flow for the TCPC models at (left) rest and under (right) exercise conditions. Black solid line, SVC flow rate; grey solid line, IVC flow rate. (Online version in colour.)

The performed multi-scale simulations evidenced that, although the local haemodynamics of the three investigated TCPC configurations were quite different, the overall cardio-circulatory behaviour was barely affected. Additionally, the energy efficiency of all three simulated surgeries was close to one. These occurrences, in contrast with the findings of a previous study [28], suggest that the systemic and pulmonary peripheral resistances probably play

a major role in Fontan patients compared with the local resistances created by different TCPC configurations. While previous studies have aimed to improve efficiency to reduce the workload on the heart, this benefit is not apparent based on the results of the present study.

## 4. Conclusions

The present study showed that a lumped parameter description of the BCPA circulation, despite not providing local haemodynamic information, can be used as a tool to set up the patient-specific parameters in the analogous multi-scale three-dimensional–zero-dimensional model. It is worth noting that an LPM alone, such as the one used in the present study, does not allow one to represent different three-dimensional TCPC configurations. Therefore, a multi-scale approach is an appropriate choice to predict the surgical outcome of the different geometrical configurations. The results obtained with multi-scale simulations revealed negligible differences among TCPC configurations in global circulatory parameters: the TCPC configuration does not seem to significantly influence the global fluid dynamics of the model. Slight improvements in performance in terms of local fluid dynamics were demonstrated by the Y-TCPC model, with better flow distribution, greater efficiency and minor power losses both at rest and in exercise. Although such results are in line with the recent literature studies [7,19], the enhancement in clinical outcome brought by a Y-graft configuration is not yet demonstrated.

The Y-graft anastomosis requires a more complex surgery; therefore further works are needed to validate results of these simulations with statistical evidence.

Future works on adaptive and autoregulatory mechanisms would make more reasonable the post-operative behaviour of similar patient-specific multi-scale models.

This study was supported by a grant from the Fondation Leducq, Paris, France. A.L.M. and W.Y. were also supported by a Beginning Grant in Aid Award from the American Heart Association, and a Burroughs Wellcome Fund Career Award at the Scientific Interface. This common work was also supported by the INRIA associated team funding. We would like to acknowledge software provided for model construction from the open source Simvascular project at simtk.org. MOCHA Investigators: Edward Bove MD and Adam Dorfman MD (University of Michigan, USA); Andrew Taylor MD, Alessandro Giardini MD, Sachin Khambadkone MD, Marc de Leval MD, Silvia Schievano PhD and T.-Y. Hsia MD (Institute of Child Health, UK); G. Hamilton Baker MD and Anthony Hlavacek (Medical University of South Carolina, USA); Francesco Migliavacca PhD, Giancarlo Pennati PhD and Gabriele Dubini PhD (Politecnico di Milano, Italy); Richard Figliola PhD and John McGregor PhD (Clemson University, USA); Alison Marsden PhD (University of California, San Diego, USA); Irene Vignon-Clementel (National Institute for Research in Computer Science and Control, France).

## References

1 de Leval, M. R. & Deanfield, J. E. 2010 Four decades of Fontan palliation. *Nat. Rev. Cardiol.* **7**, 520–527. (doi:10.1038/nrcardio.2010.99)

2 de Leval, M. R., Kilner, P., Gewillig, M. & Bull, C. 1988 Total cavopulmonary connection: a logical alternative to atriopulmonary connection for complex Fontan operations. Experimental studies and early clinical experience. *J. Thorac. Cardiovasc. Surg.* **96**, 682–695.

3 Haller, J. A. 1966 Experimental studies on permanent bypass of the right heart. *Surgery* **59**, 1128–1132.

4 de Leval, M. R., Dubini, G., Migliavacca, F., Jalali, H., Camporini, G., Redington, A. & Pietrabissa, R. 1996 Use of computational fluid dynamics in the design of surgical procedures: application to the study of competitive flows in cavopulmonary connections. *J. Thorac. Cardiovasc. Surg.* **111**, 502–513. (doi:10.1016/S0022-5223(96)70302-1)

5 Dubini, G., de Leval, M. R., Pietrabissa, R., Montevecchi, F. M. & Fumero, R. 1996 A numerical fluid mechanical study of repaired congenital heart defects. Application to the total cavopulmonary connection. *J. Biomech.* **29**, 111–121. (doi:10.1016/0021-9290(95)00021-6)

6 Soerensen, D. D., Pekkan, K., de Zelicourt, D., Sharma, S., Kanter, K., Fogel, M. & Yoganathan, A. P. 2007 Introduction of a new optimized total cavopulmonary connection. *Ann. Thorac. Surg.* **83**, 2182–2190. (doi:10.1016/j.athoracsur.2006.12.079)

7 Marsden, A. L., Bernstein, A. J., Reddy, V. M., Shadden, S. C., Spilker, R. L., Chan, F. P., Taylor, C. A. & Feinstein, J. A. 2009 Evaluation of a novel Y-shaped extracardiac Fontan baffle using computational fluid dynamics. *J. Thorac. Cardiovasc. Surg.* **137**, 394–403. (doi:10.1016/j.jtcvs.2008.06.043)

8 DeGroff, C. G. 2008 Modeling the Fontan circulation: where we are and where we need to go. *Pediatr. Cardiol.* **29**, 3–12. (doi:10.1007/s00246-007-9104-0)

9 Vignon-Clementel, I. E., Marsden, A. L. & Feinstein, J. A. 2010 A primer on computational simulation in congenital heart disease for the clinician. *Prog. Pediatr. Cardiol.* **30**, 3–13. (doi:10.1016/j.ppedcard.2010.09.002)

10 Vignon-Clementel, I. E., Figueroa, C. A., Jansen, K. E. & Taylor, C. A. 2010 Outflow boundary conditions for 3D simulations of non-periodic blood flow and pressure fields in deformable arteries. *Comput. Methods Biomech. Biomed. Eng.* **13**, 625–640. (doi:10.1080/10255840903413565)

11 Troianowski, G., Taylor, C. A., Feinstein, J. A. & Vignon-Clementel, I. E. In press. Three-dimensional simulations in Glenn patients: clinically based boundary conditions, hemodynamic results and sensitivity to input data. *J. Biomech. Eng.*

12 Pekkan, K. *et al.* 2005 Total cavopulmonary connection flow with functional left pulmonary artery stenosis: angioplasty and fenestration *in vitro*. *Circulation* **112**, 3264–3271. (doi:10.1161/CIRCULATIONAHA.104.530931)

13 Socci, L. *et al.* 2005 Computational fluid dynamics in a model of the total cavopulmonary connection reconstructed using magnetic resonance images. *Cardiol. Young* **15**(Suppl. 3), 61–67. (doi:10.1017/S1047951105001666)

14 Marsden, A. L., Vignon-Clementel, I. E., Chan, F. P., Feinstein, J. A. & Taylor, C. A. 2007 Effects of exercise and respiration on hemodynamic efficiency in CFD simulations of the total cavopulmonary connection. *Ann. Biomed. Eng.* **35**, 250–263. (doi:10.1007/s10439-006-9224-3)

15 Yang, W., Vignon-Clementel, I. E., Troianowski, G., Reddy, V. M., Feinstein, J. A. & Marsden, A. L. In press. Hepatic blood flow distribution and performance in traditional and Y-graft Fontan geometries: a case series computational fluid dynamics study. *J. Thorac. Cardiovasc. Surg.*

16 Kim, H. J., Vignon-Clementel, I. E., Coogan, J. S., Figueroa, C. A., Jansen, K. E., Taylor, C. A. 2010 Patient-specific modeling of blood flow and pressure in human coronary arteries. *Ann. Biomed. Eng.* **38**, 3195–3209. (doi:10.1007/s10439-010-0083-6)

17 Kim, H. J., Jansen, K. E., Taylor, C. A. 2010 Incorporating autoregulatory mechanisms of the cardiovascular system in three-dimensional finite element models of arterial blood flow. *Ann. Biomed. Eng.* **38**, 2314–2330. (doi:10.1007/s10439-010-9992-7)

18 Wilson, N., Wang, K., Dutton, R. & Taylor, C. A. 2001 A software framework for creating patient specific geometric models from medical imaging data for simulation based medical planning of vascular surgery. In *Medical image computing and computer-assisted intervention* (eds W. J. Niessen & M. A. Viergever). Lecture Notes in Computer Science, vol. 2208, pp. 449–456. Berlin, Germany: Springer. (doi:10.1007/3-540-45468-3_54)

19 Yang, W. G., Feinstein, J. A. & Marsden, A. L. 2010 Constrained optimization of an idealized Y-shaped baffle for the Fontan surgery at rest and exercise. *Comput. Methods Appl. Mech. Eng.* **199**, 2135–2149. (doi:10.1016/j.cma.2010.03.012)

20 Spilker, R. L., Feinstein, J. A., Parker, D. W., Reddy, V. M. & Taylor, C. A. 2007 Morphometry-based impedance boundary conditions for patient-specific modeling of blood flow in pulmonary arteries. *Ann. Biomed. Eng.* **35**, 546–559. (doi:10.1007/s10439-006-9240-3)
21 Pennati, G., Migliavacca, F., Dubini, G., Pietrabissa, R. & de Leval, M. R. 1997 A mathematical model of the circulation in the presence of the bidirectional cavoplumonary anastomosis in children with univentricular heart. *Med. Eng. Phys.* **19**, 223–234. (doi:10.1016/S1350-4533(96)00071-9)
22 Pennati, G., Migliavacca, F., Dubini, G., Pietrabissa, R., Fumero, R. & de Leval, M. R. 2000 Use of mathematical model to predict hemodynamics in cavopulmonary anastomosis with persistent forward flow. *J. Surg. Res.* **89**, 43–52. (doi:10.1006/jsre.1999.5799)
23 Migliavacca, F., Pennati, G., Dubini, G., Fumero, R., Pietrabissa, R., Urcelay, G., Bove, E. L., Hsia, T. Y. & de Leval, M. R. 2001 Modeling of the Norwood circulation: effects of shunt size, vascular resistances, and heart rate. *Am. J. Physiol. Heart Circ. Physiol.* **280**, H2076–H2086.
24 Pennati, G. & Fumero, R. 2000 Scaling approach to study the changes through the gestation of human fetal cardiac and circulatory behaviors. *Ann. Biomed. Eng.* **28**, 442–452. (doi:10.1114/1.282)
25 Pittaccio, S., Migliavacca, F., Pennati, G., Dubini, G. & de Leval, M. R. 2003 A lumped parameter model for the study of the venous return in the total cavo-pulmonary connection. In *Proc. 2003 Summer Bioengineering Conf., Key Biscayne, FL, 25–29 June 2003* (eds L. J. Soslowsky, T. C. Skalak, J. S. Wayne & G. A. Livesay), pp. 335–336. New York, NY: ASME.
26 Snyder, M. F. & Rideout, V. C. 1969 Computer simulation studies of the venous circulation. *IEEE Trans. Biomed. Eng.* **BME-16**, 325–334. (doi:10.1109/TBME.1969.4502663)
27 Migliavacca, F., Balossino, R., Pennati, G., Dubini, G., Hsia, T. Y., de Leval, M. R. & Bove, E. L. 2006 Multiscale modelling in biofluidynamics: application to reconstructive paediatric cardiac surgery. *J. Biomech.* **39**, 1010–1020. (doi:10.1016/j.jbiomech.2005.02.021)
28 Sundareswaran, K. S., Pekkan, K., Dasi, L. P., Whitehead, K., Sharma, S., Kanter, K. R., Fogel, M. A. & Yoganathan, A. P. 2008 The total cavopulmonary connection resistance: a significant impact on single ventricle hemodynamics at rest and exercise. *Am. J. Physiol. Heart Circ. Physiol.* **295**, H2427–H2435. (doi:10.1152/ajpheart.00628.2008)
29 Pennati, G., Corsini, C., Cosentino, D., Hsia, T.-Y., Luisi, V. S., Dubini, G. & Migliavacca, F. 2011 Boundary conditions of patient-specific fluid dynamics modelling of cavopulmonary connections: possible adaptation of pulmonary resistance results in a critical issue for a virtual surgical planning. *Interface Focus* **1**, 297–307. (doi:10.1098/rsfs.2010.0021)